Biomedical Optics EXPRESS

Mechanical assessment of bovine pericardium using Müeller matrix imaging, enhanced backscattering and digital image correlation analysis

Natanael Cuando-Espitia,* Francisco Sánchez-Arévalo, and Juan Hernández-Cordero

Instituto de Investigaciones en Materiales, Universidad Nacional Autónoma de México, A.P. 70-360, Cd. Universitaria, México D.F. 04510, Mexico

*natanael@iim.unam.mx

Abstract: Mechanical characterization of tissue is an important but complex task. We demonstrate the simultaneous use of Mueller matrix imaging (MMI), enhanced backscattering (EBS) and digital image correlation (DIC) in a bovine pericardium (BP) tensile test. The interest in BP relies on its wide use as valve replacement and biological patch. We show that the mean free path (MFP), obtained through EBS measurements, can be used as an indicator of the anisotropy of the fiber ensemble. Our results further show a good correlation between retardance images and displacement vector fields, which are intrinsically related with the fiber interaction within the tissue.

OCIS codes: (170.0170) Medical optics and biotechnology; (170.0110) Imaging systems; (170.6935) Tissue characterization.

References and links

1. Organ Procurement and Transplantation Network (OPTN) and Scientific Registry of Transplant Recipients, (SRTR). OPTN/SRTR 2012 Annual Data Report. Rockville, MD: Department of Health and Human Services, Health Resources and Services Administration; 2014.
2. X. Li, Y. Guo, K. R. Ziegler, L. S. Model, S. D. D. Eghbalieh, R. A. Brenes, S. T. Kim, C. Shu, and A. Dardik, "Current usage and future directions for the bovine pericardial patch," Ann. Vasc. Surg. **25**(4), 561–568 (2011).
3. K. Hammermeister, G. K. Sethi, W. G. Henderson, F. L. Grover, C. Oprian, and S. H. Rahimtoola, "Outcomes 15 years after valve replacement with a mechanical versus a bioprosthetic valve: Final report of the Veterans Affairs randomized trial," J. Am. Coll. Cardiol. **36**(4), 1152–1158 (2000).
4. J. H. Cyriax, *Diagnosis of soft tissue lesions (Vol. 1)* (Elsevier Health Sciences, 1982).
5. F. M. Sánchez-Arévalo, M. Farfán, D. Covarrubias, R. Zenit, and G. Pulos, "The micromechanical behavior of lyophilized glutaraldehyde-treated bovine pericardium under uniaxial tension," J. Mech. Behav. Biomed. Mater. **3**(8), 640–646 (2010).
6. N. Ghosh, M. F. G. Wood, S. H. Li, R. D. Weisel, B. C. Wilson, R.-K. Li, and I. A. Vitkin, "Mueller matrix decomposition for polarized light assessment of biological tissues," J. Biophotonics **2**(3), 145–156 (2009).
7. N. Cuando-Espitia, F. M. Sánchez-Arévalo, and J. Hernández-Cordero, "Enhanced backscattering measurements in bovine pericardium tensile tests," in Latin America Optics and Photonics Conference, OSA Technical Digest, paper LTh4A.22 (2014).
8. P. I. Okagbare, D. Begun, M. Tecklenburg, A. Awonusi, S. A. Goldstein, and M. D. Morris, "Noninvasive Raman spectroscopy of rat tibiae: approach to in vivo assessment of bone quality," J. Biomed. Opt. **17**(9), 090502 (2012).
9. J. C. Briones-Herrera, N. Cuando-Espitia, F. M. Sánchez-Arévalo, and J. Hernández-Cordero, "Evaluation of mechanical behavior of soft tissue by means of random laser emission," Rev. Sci. Instrum. **84**(10), 104301 (2013).
10. V. Turzhitsky, J. D. Rogers, N. N. Mutyal, H. K. Roy, and V. Backman, "Characterization of light transport in scattering media at sub-diffusion length scales with Low-coherence Enhanced Backscattering," IEEE J. Sel. Top. Quantum Electron. **16**(3), 619–626 (2010).
11. A. Lagendijk, "Observation of weak localization of light in a random medium," Phys. Rev. Lett. **55**(24), 2692–2695 (1985).
12. E. Akkermans, P. E. Wolf, and R. Maynard, "Coherent backscattering of light by disordered media: Analysis of the peak line shape," Phys. Rev. Lett. **56**(14), 1471–1474 (1986).

#241610 Received 22 May 2015; revised 2 Jul 2015; accepted 3 Jul 2015; published 20 Jul 2015

13. S. Lu and R. Chipman, "Interpretation of Mueller matrices based on polar decomposition," J. Opt. Soc. Am. A **13**(5), 1106–1113 (1996).
14. R. Azzam, "Propagation of partially polarized light through anisotropic media with or without depolarization: A differential 4 × 4 matrix calculus," J. Opt. Soc. Am. **68**(12), 1756–1767 (1978).
15. R. Ossikovski, "Differential matrix formalism for depolarizing anisotropic media," Opt. Lett. **36**(12), 2330–2332 (2011).
16. C. E. Willert and M. Gharib, "Digital particle image velocimetry," Exp. Fluids **10**(4), 181–193 (1991).
17. F. M. Sánchez-Arévalo and G. Pulos, "Use of digital image correlation to determine the mechanical behavior of materials," Mater. Charact. **59**(11), 1572–1579 (2008).
18. F. M. Sánchez-Arévalo, T. García-Fernández, G. Pulos, and M. Villagrán-Muniz, "Use of digital speckle pattern correlation for strain measurements in a CuAlBe shape memory alloy," Mater. Charact. **60**(8), 775–782 (2009).
19. P. Fratzl, *Collagen: Structure and Mechanics* (Springer, 2008).
20. R. Puxkandl, I. Zizak, O. Paris, J. Keckes, W. Tesch, S. Bernstorff, P. Purslow, and P. Fratzl, "Viscoelastic properties of collagen: synchrotron radiation investigations and structural model," Philos. Trans. R. Soc. Lond. B Biol. Sci. **357**(1418), 191–197 (2002).
21. M. J. Ju and S. Tang, "Usage of polarization-sensitive optical coherence tomography for investigation of collagen cross-linking," J. Biomed. Opt. **20**(4), 046001 (2015).

1. Introduction

Heart transplant procedures cover only a small portion of the actual needs of patients with heart related problems. In 2012, and only in the US, heart donation rates remained flat at 3.5 donations per 1000 deaths [1]. Most of the top causes of heart related diseases, such as aortic and mitral valve disorders, require valve replacement using bioprosthetic or mechanical heart valves. Bovine pericardium (BP) is a widely used soft tissue for medical applications such as valve replacement [2]. Among other interesting features, patients with BP-based valves usually do not need a life-long anticoagulation treatment [3]. Although BP is commonly used in medical applications, the knowledge to fully predict its behavior once inside the human body is still unclear, and long-term results are not fully documented. In general, *in vivo* soft tissue characterization methods are limited and very expensive [4].

Recently, digital image correlation (DIC) and Müeller matrix imaging (MMI) have been reported as useful techniques for extracting information from biological tissue [5,6]. Similarly, enhanced backscattering (EBS) measurements have shown to provide information of structural changes in soft tissue during mechanical tests [7]. In general, optical characterization methods allow for performing non-contact and less invasive procedures, particularly those intended to obtain mechanical features of soft tissue. Moreover, optical techniques for soft tissue tests have the potential to be integrated with fiber optics technology and lead to applications such as *in vivo* early tissue diagnosis [8]. In this paper, we report on the application of MMI for uniaxial tensile tests of BP previously fixed with glutaraldehyde. Our experiments are performed using a setup specifically designed for mechanical testing of soft tissue [9]. This allows for incorporating optical techniques for tissue analysis during uniaxial tension tests. In particular, data from DIC, EBS and MMI are obtained simultaneously thus providing information regarding structural changes of the tissue samples during the tensile test. In this way, the mechanical properties of the tissue can be readily correlated with the optical measurements.

2. Materials and methods

2.1 Experimental setup

The experimental setup consists of a mechanical testing device designed to perform tensile tests on thin and soft materials [9]. This mechanical "minitester" further incorporates optical elements to acquire information for EBS and MMI measurements. As depicted schematically in Fig. 1, a set of circular polarizers is used to generate and analyze the states of polarization required for MMI [6]. Images are acquired via a long working distance microscope and a CCD camera, both arranged to register the beam coming out from the sample in the forward direction (green arrows in Fig. 1). Illumination for both, MMI and EBS, is performed with a

#241610 Received 22 May 2015; revised 2 Jul 2015; accepted 3 Jul 2015; published 20 Jul 2015

pulsed, frequency-doubled Nd:YAG laser at 532nm, with a spot diameter of approximately 0.5 cm.

A second CCD camera placed as shown on the right side of Fig. 1 registers data for EBS measurements. After interacting with the sample, the scattered light in the backward direction passes through the circular polarizer for filtering of specular reflections. The EBS cone is then registered using a lens with a focal length of 45 mm and the 1024x768 CCD. This configuration provides a resolution of 0.1 mrad with no moving parts once adjustments on the alignment have been completed [10].

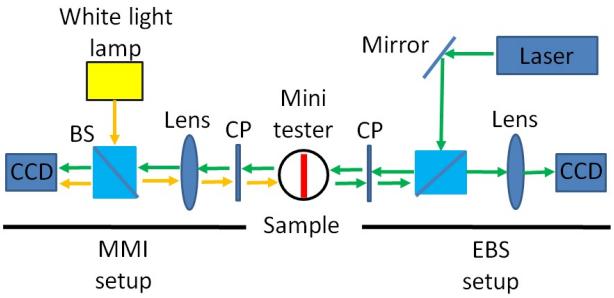

Fig. 1. Experimental setup: data for MMI, DIC and EBS are acquired during a single uniaxial test. The setup includes circular polarizers (CP), a beam splitter (BS), a laser and a white light source for illumination as well as two CCD cameras (see text).

Conventional images are recorded using white light illumination for subsequent processing using DIC. The mechanical "minitester," CCD cameras and laser trigger are controlled and synchronized with a PC via a Virtual Instrument (VI) programmed in *LabVIEW*. The VI is set to start the test in a sequential manner; first, the sample is elongated in steps of 200 μm, simultaneously acquiring white light images and data such as applied force and displacement for subsequent mechanical analysis. In order to avoid relaxation effects in the BP sample during MMI measurements, the VI is set to pause during 4 minutes once the applied load reaches a preset value. This relaxation time was determined experimentally through preliminary measurements showing that after 4 minutes, relaxation effects are negligible for MMI and EBS analysis. After this pause, the Nd:YAG laser is triggered to launch 10 pulses per each of the 16 combinations on the circular polarizers required for the Müeller matrix for the corresponding loading condition. Subsequently, the laser is triggered again to launch 10 pulses for acquiring images for EBS analysis. The VI then starts the loading procedure again for data and image acquisition under different loading conditions.

2.1 Sample preparation

As other connective tissues, BP has a complex structure based on three layers: the serosa, the fibrosa and the epipericardial connective tissue layer [2]. The fibrosa layer is mainly made of wavy bundles of collagen fibers and elastin; the properties of this layer provide bovine pericardium with the appropriate features for its clinical use as a biological patch and for heart valve replacement [2,3]. For our experiments, pericardial sacs from 18 month-old calves were collected fresh from a local slaughterhouse. Sample sheets of selected sacs were cut and hung in custom-built frames; subsequently, they were cross-linked with glutaraldehyde (GA). The fixation process was carried out during 24 hours at 4°C, using 0.5% GA in 0.1 M phosphate buffered saline solution with a pH of 7.4 [5]. Next, the sheets were washed in distilled water and subsequently cut with a special jig, according to the ASTM D1708 standard, to obtain samples with a dog bone shape. Finally, the samples were immersed and stored in a glycerin solution until the experiment was performed.

#241610 Received 22 May 2015; revised 2 Jul 2015; accepted 3 Jul 2015; published 20 Jul 2015

2.3 Mean free path measurements (EBS)

According to EBS theory, when light interacts with multiple scattering media a twofold enhancement in the diffuse intensity appears in the exact backward direction. The factor of two arises from photons going over time-reversed paths, which constructively interfere in the direction of backscattering [11,12]. Out from the exact backscattering direction, the enhancement decreases inversely proportional to the mean free path (MFP), forming an angular distribution that decays to the diffusive intensity. For non-absorbing media, the intensity α near the backscattering direction as a function of the solid angle θ is given by [12]:

$$\alpha(\theta) = \frac{3}{8\pi}\left[1 + \frac{2z_0}{l} + \frac{1}{(1+ql)^2}\left(1 + \frac{1-e^{-2qz_0}}{ql}\right)\right] \quad (1)$$

In this expression, $q = 2\pi\theta/\lambda$, l is the photon mean free path; z_0 is given by the boundary conditions and for a plane geometry $z_0 \sim 0.7\, l$ [12]. Equation (1) shows that for fixed boundary conditions and wavelength λ, the shape of the EBS cone is fully described by the mean free path (MFP), which is a measure of the turbidity of the sample. This allows for obtaining an experimental measurement of the MFP for a sample upon evaluation of the width of the angular distribution of the backscattered intensity. In our experiments, the intensity recorded in each pixel of the CCD was mapped to the scattering angle considering both, the pixel width and the focal length as described in [10]. Subsequently, Eq. (1) was fitted to the experimental data to obtain the MFP (i.e., l) in terms of the wavelength and the width of the EBS cone.

2.4 Experimental Müeller matrix decomposition

Müeller calculus is a well-established technique for homogeneous transparent media. Nevertheless, when dealing with inhomogeneous materials such as tissue, the elements of the experimental Müeller matrix can mislead to a non-physical behavior of the material [6]. Scattering, depolarization and inhomogeneity of the material must be considered in data analysis in order to obtain the relevant physical parameters from the matrix. Two methods have been reported aiming at solving this difficulty: the so-called polar decomposition [13], and the differential matrix formalism [14]. We used the extension of the differential matrix formalism for depolarizing anisotropic media [15], in which the spatial derivative of the Müeller matrix along the propagation axis follows the relation:

$$\frac{d\mathbf{M}(z)}{dz} = \mathbf{m}\mathbf{M}(z) \quad (2)$$

$\mathbf{M}(z)$ represents the position dependent Müeller matrix and $\mathbf{m}$ is the differential matrix. Equation (2) implies that the optical effect caused by the material scales with the sample thickness [14,15]. For the boundary condition $\mathbf{M}(z = 0) = \mathbf{I}$, where $\mathbf{I}$ is the identity matrix, the solution of Eq. (2) has the form $\mathbf{M} = \exp(d\mathbf{m})$, in which d is the path traveled by the light beam. In our experiments, we construct the experimental Müeller matrix using the different combinations of the circular polarizers for a sample of thickness d. Each pixel in the acquired images thus has an associated Müeller matrix; these are subsequently used to obtain the differential matrix $\mathbf{m}$ using Jordan decomposition. The Müeller matrix provides information such as linear retardance (δ), optical rotation and average depolarization [6]. We focus on the linear retardance, which is related to the stress-induced changes in refractive index.

2.5 DIC analysis

Digital image correlation is a full-field and non-contact technique to measure displacement/strain vector fields (DVFs) on the surface of materials. With the series of acquired images during the mechanical tests, the DVFs $\boldsymbol{u}_k\,(x_k, y_k)$ and $\boldsymbol{v}_k\,(x_k, y_k)$ between pair of images were calculated by using the Willert and Gharib algorithm [16]. Here $\boldsymbol{u}$ and $\boldsymbol{v}$ represent the displacement vectors of the object or region of interest in the x and y directions,

#241610 Received 22 May 2015; revised 2 Jul 2015; accepted 3 Jul 2015; published 20 Jul 2015

respectively [17,18]. The position coordinates in each image are represented by x and y and subindex k indicates the corresponding object/region of interest, which is defined as an area of 64 × 64 pixels. Hence, a full image is divided in subimages (64 × 64 pixels) used to perform the DIC analysis yielding the DVF at throughout the full image for a given loading condition. The in-plane strains in the sample were evaluated by minimizing the errors of a six parameters linear model (typically used in linear elasticity theory) and previously used in other materials including bovine pericardium [17,18]. This minimization yields the values for the normal strain in the x and y directions (ε_x and ε_y), translation, shear strain (ε_{xy}), and in-plane rotation within the analyzed region of the sample [18].

3. Results and discussion

Macroscopically, BP can be seen as an ensemble of fibers that tend to align in the direction of the stress axis during the mechanical test [5]. Before rupture, the tissue exhibits three main regions in the stress-elongation ratio curve. In the first region, the elongation ratio increases with small changes in the applied stress as depicted in Fig. 2. After a certain value of the elongation ratio, some of the fibers start to align, and a highly nonlinear transition region appears. Finally, when most of the fibers are aligned, a third region showing a linear response to elongation can be identified. As shown in Fig. 2(b), these three regions were obtained in our experiments for elongation ratios of 0.0-0.15 (region I), 0.15-0.3 (region II) and 0.3-0.4 (region III). Changes in the fiber alignment for different loading conditions are evident in the images shown in Fig. 2(a): as the load increases, the fibers tend to align along the direction of the force applied to the sample.

Fiber alignment modifies the scattering conditions within the tissue thereby affecting the MFP. As shown in Fig. 2, the resulting MFP measured through EBS varies under different loading conditions. The preset values for the load on the sample were set to obtain data for EBS within the three regions of the stress-elongation curve. As seen in the figure, the MFP exhibits an inflexion point within region II, indicating a transition zone in which the collagen fibers of the tissue begin to align. These ordered-disordered transitions are characteristic for collagen fibers based tissue [19]. Within region III, both the stress and MFP show a similar behavior increasing with the elongation ratio. This can be related to an increase in scatterers per unit volume as the elongation ratio increases. Upon loading the BP sample, the tissue experiences a contraction along the transversal direction owing to the Poison ratio. This contraction leads to a rearrangement of the collagen fibers along the horizontal direction thus increasing the number of scatterers (fibers) per unit of volume. Hence, the scattering force within the sample increases along with the MFP [10]. This may be related to the intrafibrillar structure of collagen, and has been directly observed during mechanical tests by means of small-angle X-ray scattering (SAXs) measurements [20]. We therefore believe that EBS measurements provide an alternative means for evaluation of intrafibrillar modifications in densely packaged collagen tissue.

#241610 Received 22 May 2015; revised 2 Jul 2015; accepted 3 Jul 2015; published 20 Jul 2015

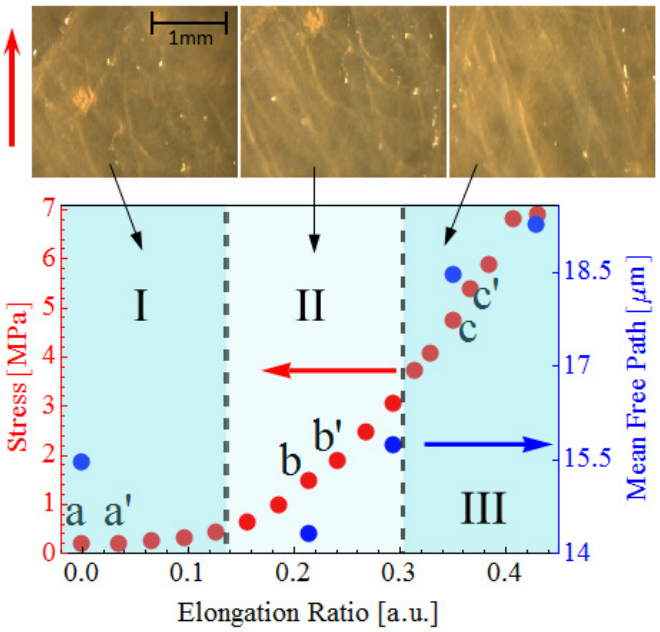

Fig. 2. Stress vs. elongation ratio curve of the BP tensile test (red points, left axis) and MFP as function of elongation ratio (blue points, right axis). The pictures show representative images for each region of the stress vs. elongation ratio curve. The arrow on the left side of the images indicates the direction of the load during the uniaxial tension test.

While the mechanical data recorded during the tests are linked to the behavior of the fibers at a macroscopic scale, EBS measurements provide information related to fiber interaction within the illuminated portion of the sample. More localized information of the tissue is provided by DIC and MMI. These provide data at the micron scale within the probed area acquired by the imaging system. The left column of Fig. 3 shows the images obtained using white light illumination of the BP sample together with the corresponding DVFs (superimposed white lines with arrow heads). By means of DIC, the DVFs are obtained upon comparing subsequent images for different loading levels [5]. In this case, we present three sets of vectors, one for each of the regions shown in the stress-elongation curve (i.e., regions I, II and II). The DVFs for each region were obtained from image pairs acquired during the elongation test; the selected points of the curve for this calculations are shown in Fig. 2 and are labeled as a-a' (region I), b-b' (region II) and c-c' (region III). For comparison, the corresponding images for the linear retardance (δ) in degrees, calculated through differential matrix decomposition, are shown in the right column of the same figure. The linear retardance for each pixel is represented in an arbitrary color scale and is shown together with the corresponding DVFs.

The DVFs in Fig. 3(a) display a larger displacement component along the perpendicular axis to the applied load. Since Fig. 3(a) corresponds to elongation conditions of region I, in which the fibers are not aligned, some compression is to be expected owing to fiber displacement during the initial elongation. The retardance image for the initial conditions (right column of Fig. 3(a)) shows a relatively regular distribution of low retardance. This is a consequence of the highly isotropic orientation of the fibers for this loading condition, where alignment is not yet achieved. Notice also that the zones with highest retardance in Fig. 3(a) tend to match the elongation components of the DVFs, suggesting that the vectors are attracted to the zones with higher retardance. For elongation ratios beyond 0.2 (region II), the DVFs exhibit a clear change as the predominant component is aligned towards the loading axis, as seen in Fig. 3(b). This alignment is associated with the appearance of high retardance

#241610 Received 22 May 2015; revised 2 Jul 2015; accepted 3 Jul 2015; published 20 Jul 2015

zones increasing the contrast of the image. In general, the DVF in Fig. 3(b) tends to run from high retardance zones to lower retardance zones as in Fig. 3(a). Finally, the DVF of Fig. 3(c) shows the characteristic hyperbolic pattern of an aligned ensemble of fibers, as expected within the linear region of the tensile test [5]. In this case the retardance image displays a spread of higher retardance zones, owing to an increased interaction among the microfibers within the tissue [19]. In general, high retardance zones tend to spread as the elongation ratio increases. Notice however that for larger loading conditions, some of the zones with low retardance seem to attract the DVFs as it is shown at lower part of Fig. 3(c). This may be attributed to buckling in the central part of the image, which has been previously reported to appear in BP tissue samples under high stress conditions [5].

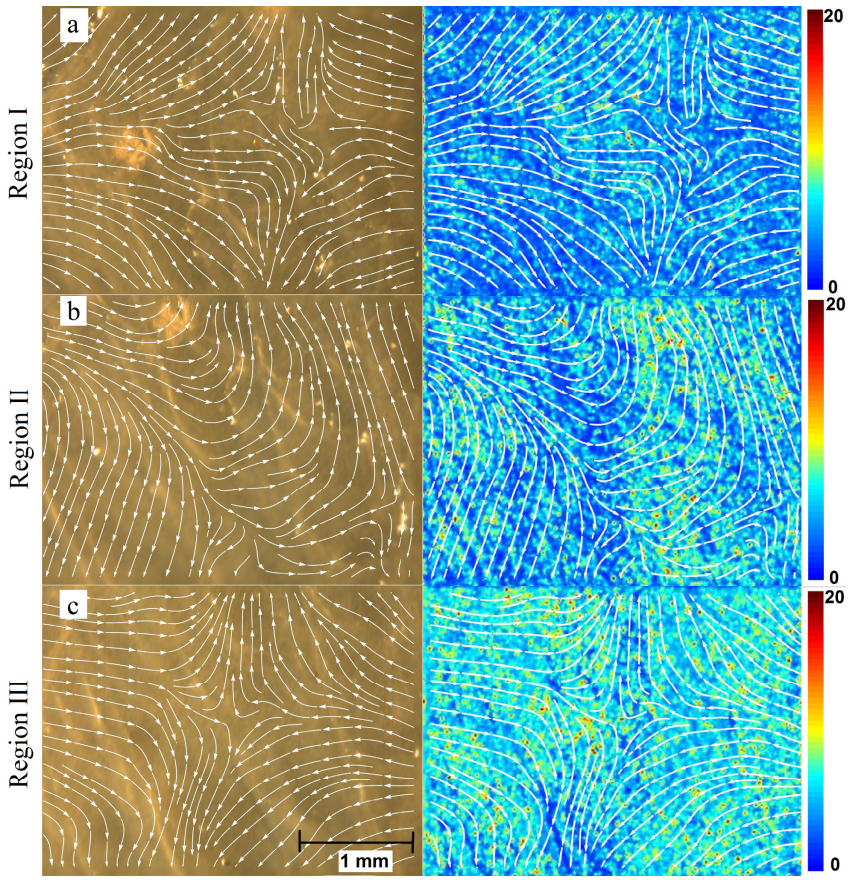

Fig. 3. Left column: white light images of the BP and their corresponding DVF. Right column: retardance images obtained from MMI analysis and their corresponding DVF. The scales for the retardance images are in degrees; each row is associated with different regions of the tensile test (see text). DVFs correlate well with retardance images obtained by means of MMI during the tensile test (Visualization 1).

Another interesting feature of the retardance images is the localized points of high retardance. These localized points reach the maximum values of the color scale and become more evident as the load increases as it is illustrated in Fig. 3. An increase in collagen fiber interactions typically leads to the rupture of cross-links between adjacent fibers [19]. Mechanical testing of BP tissue has shown to generate cross-linking rupture creating localized zones of high shear stress [5]. This condition is achieved under the loading conditions shown in region III of Fig. 2 and leads to changes in birefringence that appear as localized zones with high retardance as shown in Fig. 3. Similar conditions have been observed when

#241610 Received 22 May 2015; revised 2 Jul 2015; accepted 3 Jul 2015; published 20 Jul 2015

studying collagen cross-linking effects in corneal tissue using polarization sensitive OCT [21].

4. Conclusions

We have demonstrated that optical measurements, in particular DIC, MMI and EBS, can be incorporated into tensile tests of BP tissue. While DIC provides information related to the interaction between the tissue matrix and the collagen fibers, MMI accounts for interfibrillar changes in the tissue structure; EBS in turn shows intrafibrillar effects during the elongation test. The proposed arrangement is thus capable to provide information at different scales during a single mechanical test. It is clear from EBS measurements that the mean free path (MFP) within the tissue sample increases with elongation. Longer MFPs are associated to the linear region of the tensile test, where fibrils are in a more compact and aligned arrangement. The displacement vector fields (DVFs) obtained by DIC show a good correlation with the retardance images calculated by means of MMI. Our observations suggest that DVFs tend to run from low retardance zones to high retardance zones, where more fiber interaction is present. Similar trends in changes of tissue structure during mechanical tests have been reported using more elaborated techniques such as OCT and SAXs. We therefore believe that incorporation of these optical tools for tissue characterization represents a promising approach for elucidating mechanical properties of materials used for biological prosthetic devices.

Acknowledgments

This work was partially supported by DGAPA-UNAM through grants PAPIIT IT100215, IT101215. Natanael Cuando-Espitia acknowledges support from CONACYT. The authors are also grateful to Professor Enrique Geffroy-Aguilar for facilitating the laser equipment used in this work.